Supplemental Table

Table S1. (Related to Figure 1) Summary of craniofacial abnormities caused by 3 groups of chemicals

Compound	ethmoid plate	mandible	skull base	annotation
Retinoic acid, all trans	absent	absent	absent	retinoid RAR agonist
Leflunomide	absent	absent	absent	pyrimidine synthesis inhibitor
PP2	absent	absent	absent; elements	Src tyrosine kinase inhibitor
TRIM	absent; dispersed	absent; ectopic	absent; ectopic	nNOS/iNOS inhibitor
GW-9662	absent; elements	absent	absent	PPAR gamma antagonist
AG-1296	absent; elements	elements	absent	c-kit/FGF/PDGF kinase inhibitor
Estradiol	absent; elements	absent; elements	absent	estrogen
Diazoxide	fused	disrupted ceratohyal	intact	potassium channels
Arachidonamide	fused	small	absent	arachidonic acid metabolite
Anandamide (18:2, n-6)	fused	small	absent	cannabinoid receptor agonist
GF-109203X	fused	absent	intact	PKC inhibitor
Geranylgeraniol	fused	elements	absent	diterpene alcohol
Pimozide	short	dysmorphic	intact	calcium channels
REV-5901	narrow; small	small	small	5-Lipoxygenase inhibitor
N-Linoleoylglycine	short	short	intact	FAAH inhibitor
Pifithrin	short	small	intact	p53 inhibitor
Fipronil	short	small	intact	Ion channel ligands (Misc.)
Prostaglandin A2	short	very small	intact	bioactive prostaglandin
6(5H)-Phenanthridinone	short	absent	intact	PARP inhibitor
BF-170	short	normal	intact	N/A
Genistein	short	dysmorphic	intact	tyrosine protein kinase inhibitor

Supplemental Figures

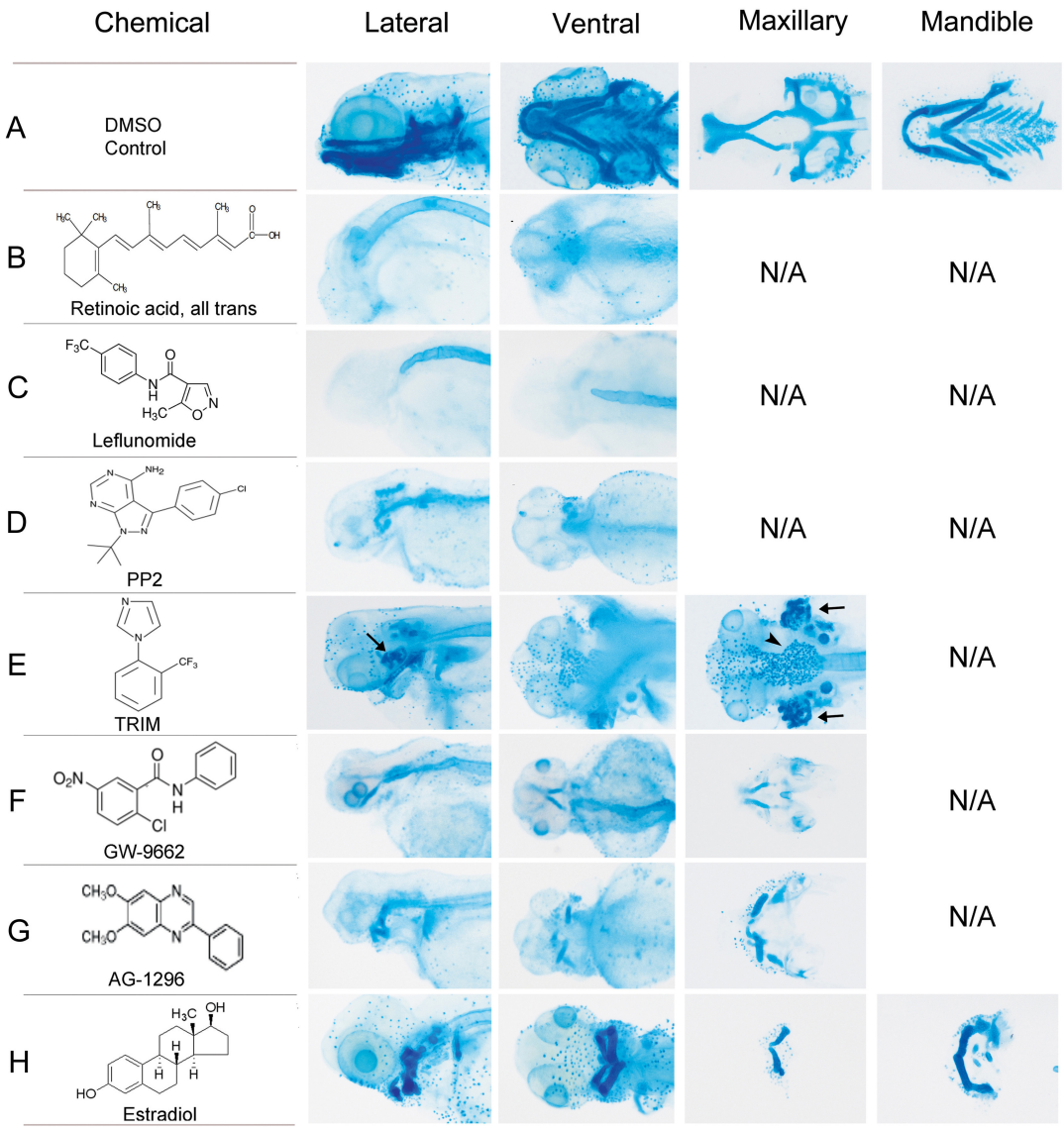

Figure S1. (Related to Figure 1) Chemical genetic screen identified small molecules that abrogate CNC and craniofacial morphogenesis. Chemical structures of retinoic acid (all trans), leflunomide, PP2, TRIM, GW-9662, AG-1296 and estradiol are shown on the left panel. Alcian blue stained cartilages of 4 dpf embryos after chemical treatment (**B-H**) were compared with DMSO control (**A**). The stained cartilaginous structures are shown by the lateral view and ventral view in general; and also by dissected neurocranium from the dorsal aspect, the pharyngeal skeleton from the ventral aspect. The deformities of the craniofacial skeleton were marked by the absence of ethmoid plate, mandible and/or skull base (or only small elements

remained). Among these, TRIM resulted in ectopic cartilage formation, which was characterized by the paired “claw-like” structure (E, arrows).

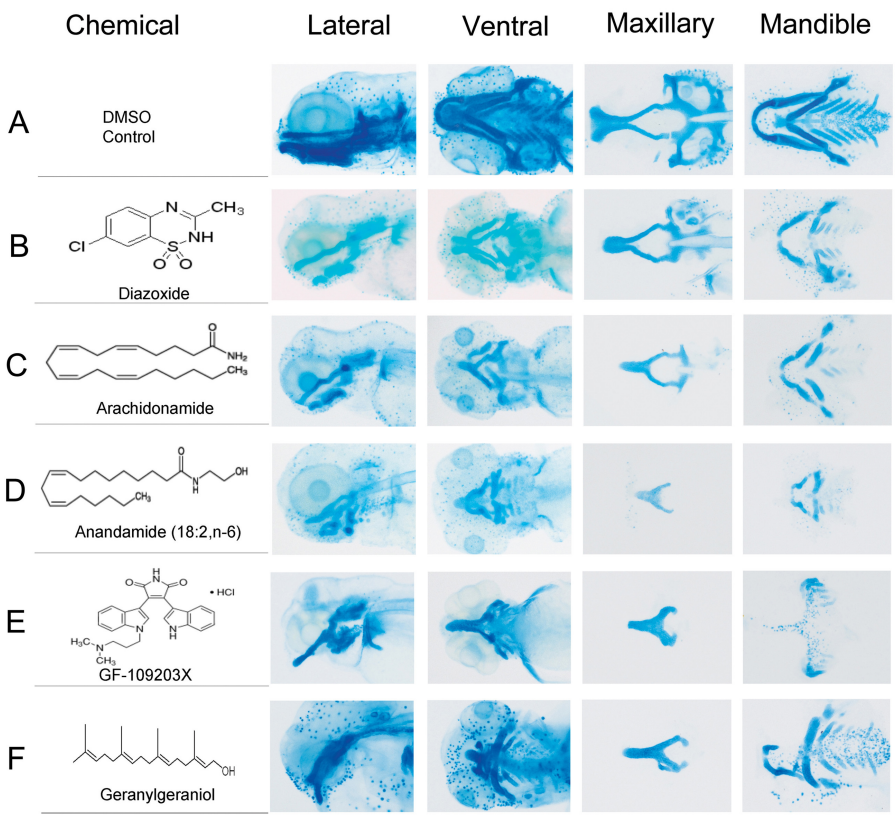

Figure S2. (Related to Figure 1) Chemicals leading to fused ethmoid plate and disrupted lower jaw structure. Alcian blue stained craniofacial cartilage are arranged in lateral, ventral and dissected views. Diazoxide, arachidonamide, anandamide, GF-109203X, and geranylgeraniol were identified from the library and classified as the second group to cause ethmoid and trabecula dysmorphogenesis. Specifically, ethmoid plate was fused at the anterior region (**B-D**) or even together fused with the trabecula (**E, F**). The pharyngeal skeleton failed to fully develop and only cartilage elements remained.

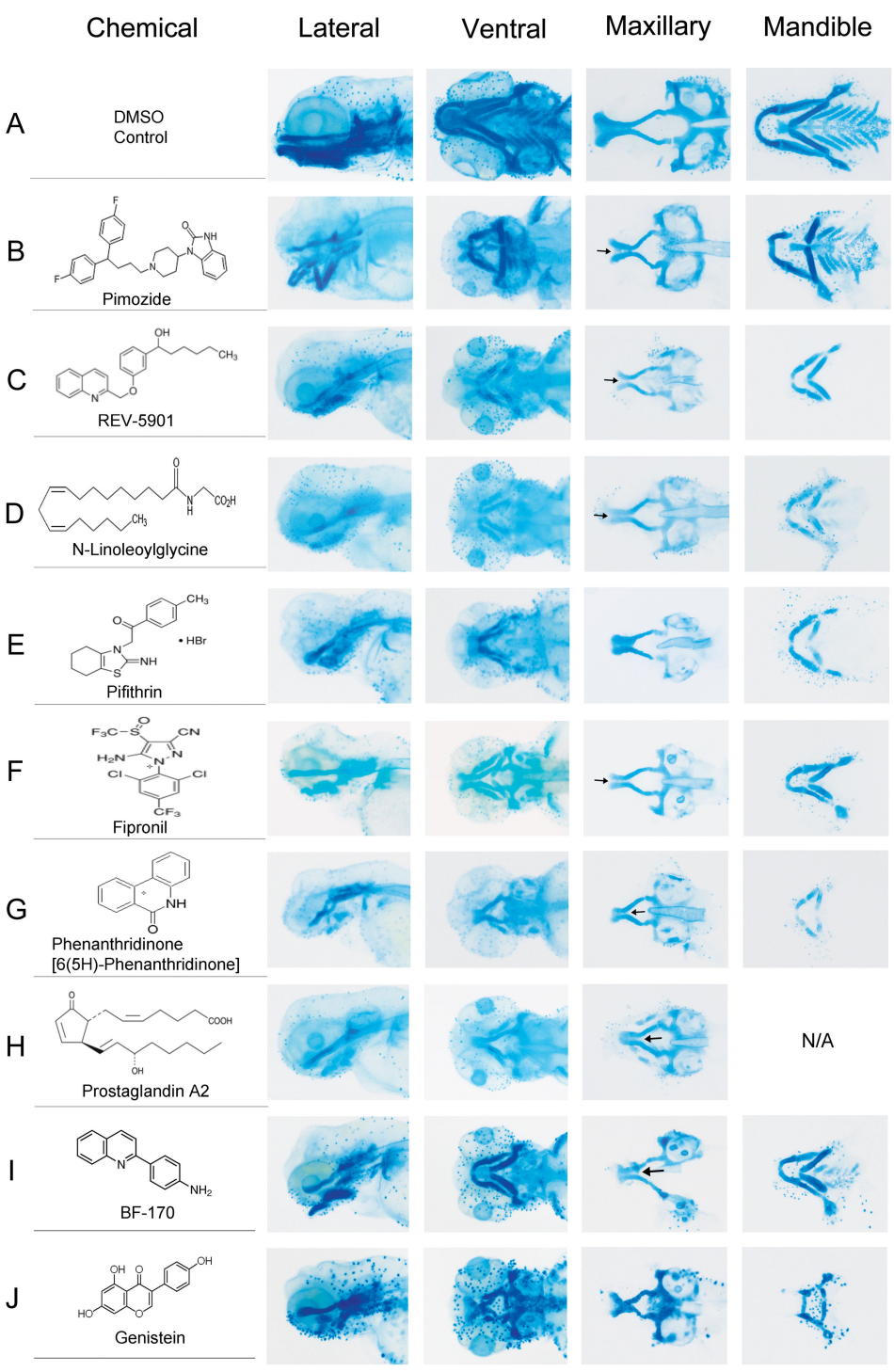

Figure S3. (Related to Figure 1) Chemicals that caused shortened but formed ethmoid plate and Meckel's cartilage. 9 compounds were identified from the library to result in short or small ethmoid plate and lower jaw, whereas the skull base was basically well developed. Arrows in B-D, and in F-I indicate the cleft or seam from the dorsal view of the dissected upper jaw.

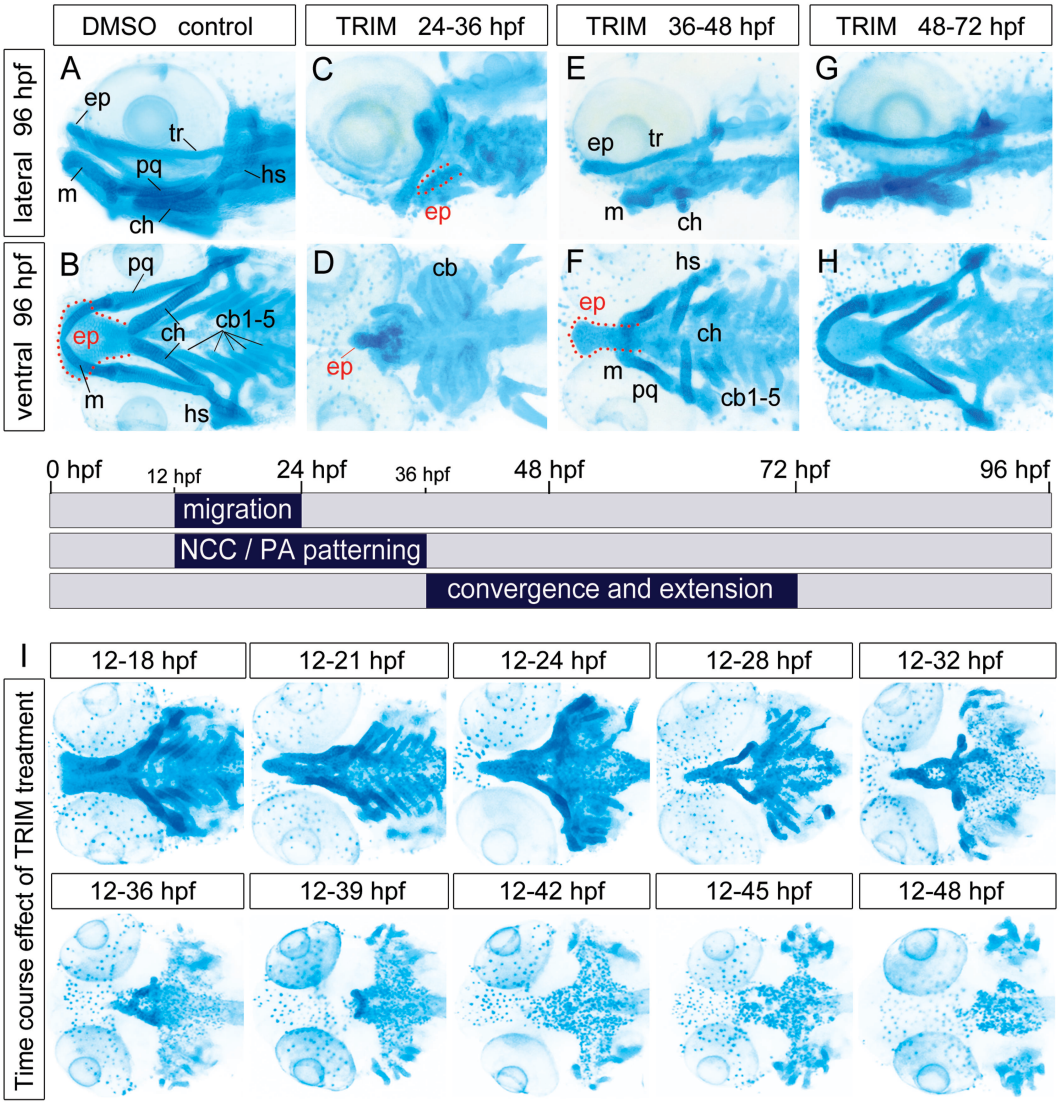

Figure S4. (Related to Figure 1) Inhibitory effect of TRIM on CNC cells is temporal and regional specific. (**A-H**) Developmental stages were sequentially blocked by TRIM, targeting PA patterning (24-36 hpf, C-D), facial prominences (36-48 hpf, E-F), convergence and extension (48-72 hpf, G-H). The resulting craniofacial skeleton was shown by Alcian blue stain at 96 hpf. (**A-B**) Normal palate development includes ethmoid plate (*ep*), trabecula (*tr*). The lower jaw elements are Meckel's (*m*), palatoquadrate (*pq*), hyosymplectic (*hs*), ceratohyal (*ch*), and ceratobranchial (*cb*). (**C-D**) TRIM treatment at 24-36 hpf resulted in malformed jaw skeleton where the ethmoid plate was short, fused and ventrally displaced, with absence of Meckel's cartilage, and paired structures resembling ceratobranchials formed in a transverse pattern. (**E-F**) TRIM treatment at 36-48hpf caused hypoplastic skeleton with a narrow ethmoid plate and

shortened lower jaw structures. (**G-H**) TRIM treatment after 48 hpf had little effect on the formation of craniofacial structures. (**I**) TRIM treatment with increasing duration from onset of CNC cell migration at 12 hpf resulted in progressive elimination of craniofacial cartilage structures. With increasing duration of TRIM, ethmoid plate and Meckel's cartilage were reduced to scattered chondrocytes and the ceratobranchials failed to form.

Figure S4. Annotation

Inhibitory effect of TRIM on CNC cells is temporal and regional specific

Our initial screen to identify TRIM as a potent craniofacial modulator was performed by 12-96 hpf exposure, during which time coordinated CNC development events such as patterning migration, convergence and extension movements all take place. To better delineate the developmental processes affected by TRIM, chemical treatments at discrete stages and graded durations were carried out. We found that TRIM treatment at 24-36 hpf, a temporal window corresponding to CNC and pharyngeal arches patterning, profoundly inhibited development of both dorsal and ventral pharyngeal skeletons. Compared to DMSO control (Fig. S4A, B), the ethmoid plate was significantly stunted and ventrally displaced, Meckel's cartilage was not formed, and what appeared to be the paired segmental ceratobranchial structures were abnormally shaped and splayed out (Fig. S4C, D). If the window of TRIM treatment was restricted to 36-48 hpf during convergence of facial prominences, the jaw structures did form but the ethmoid plate and the lower jaw failed to extend (Fig. S4E, F). However, TRIM treatment after 48 hpf during extension of jaw structures exerted modest effect (Fig. S4G, H). Therefore, the CNC cell migration and patterning events before 36 hpf appear to be most susceptible to TRIM effect, whereas later treatment after 48 hpf did not significantly impact the extension mechanism in craniofacial morphogenesis. Meanwhile, TRIM treatment during gastrulation does not affect craniofacial morphogenesis (data not shown).

Dynamic and directional cell migration is one of the major properties that defines CNC. In zebrafish, this occurs beginning at 10-12 hpf, and ends around 20-24 hpf. To better delineate early embryonic events that are susceptible to TRIM, we also performed TRIM treatment with increasing duration, beginning at the onset of CNC migration from 12 hpf (5-9 somites) to 48 hpf. When the duration of TRIM treatment increased, we observed progressive elimination of

cranial skeletal structures, where development of the upper and lower jaw was gradually ablated until the ceratobranchials were also affected (Fig. S4I). Notably, as the duration of TRIM treatment increased from 12-18 hours to 12-48 hours, we observed that the more anterior CNC cells were more susceptible to TRIM effect, as structures derived from the anterior migrating stream around the eye and the first PA (ethmoid plate and Meckel's cartilage) were more profoundly abrogated than the more posterior arch structures (ceratobranchials), suggesting an anterior-posterior patterning defect (Fig. S4I). These results collectively demonstrate that TRIM's effect on CNC development is temporal and regional specific, with most profound inhibition during periods of CNC migration, patterning, and convergence morphogenesis.

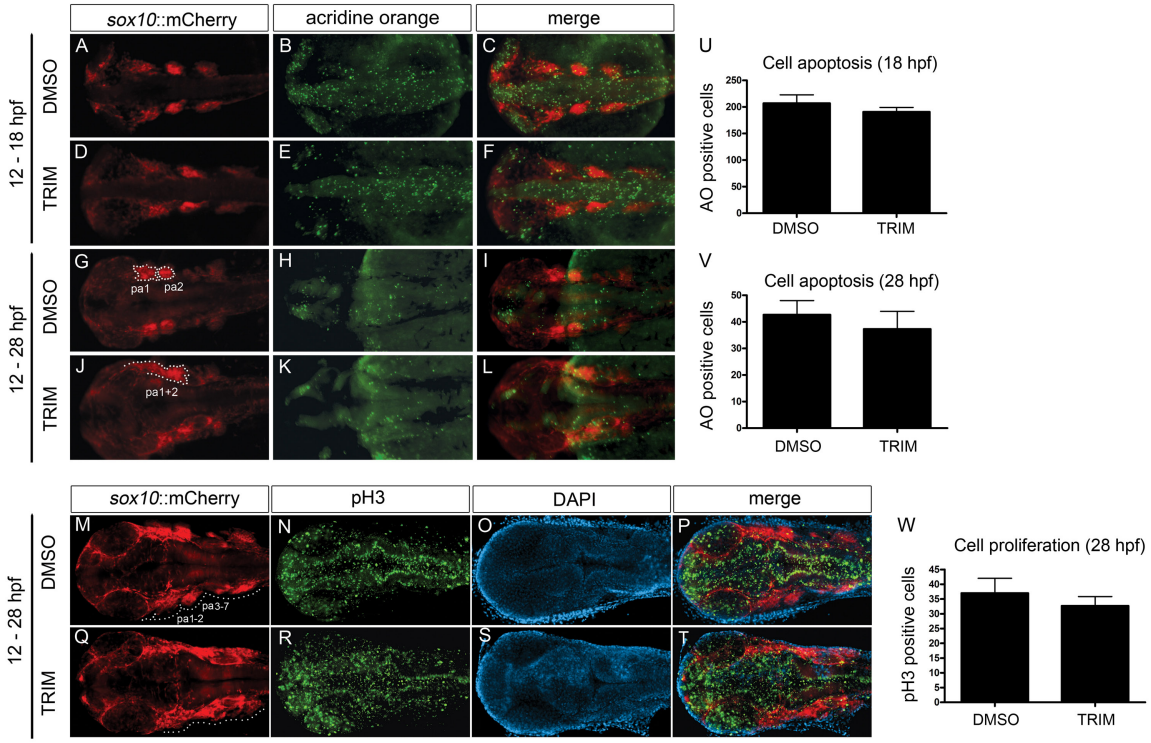

Figure S5. (Related to Figure 4) Changes in cell death and proliferation do not explain the loss of pharyngeal structures. (**A-L**) *Tg (sox10::mCherry)* embryos with acridine orange (AO) labels apoptotic cell death (green) under the treatment of DMSO or TRIM. Neither active migrating CNC cells at 18 hpf (A-F) nor post-migratory CNC cells at 28 hpf (G-L) exhibits increased apoptosis. However, with TRIM treatment, disorganized boundary among pharyngeal arches can be detected at 28 hpf compared to the distinct patterning in DMSO (G, J; M, Q, also illustrated in Fig. 3 A). (**M-T**) Cell proliferation was assayed by staining *Tg (sox10::mCherry)* embryos with phosphor-histone H3 (pH3, green). Embryos were counterstained with DAPI to label nuclei. There was no significant difference in $pH3^+$ cells in all pharyngeal arches between DMSO and TRIM-treated embryos at 28 hpf. (U-W) Quantification of AO^+ cells and $pH3^+$ cells in CNC by scoring positive signals from three different focus depths (Z-stack). Phospho-histone H3 antibody labeling was performed using anti-phosphohistone H3 rabbit polyclonal antibody (Ser10) (1:500, Millipore) and anti-rabbit Alexa Fluor 488 (1:1000, Invitrogen).

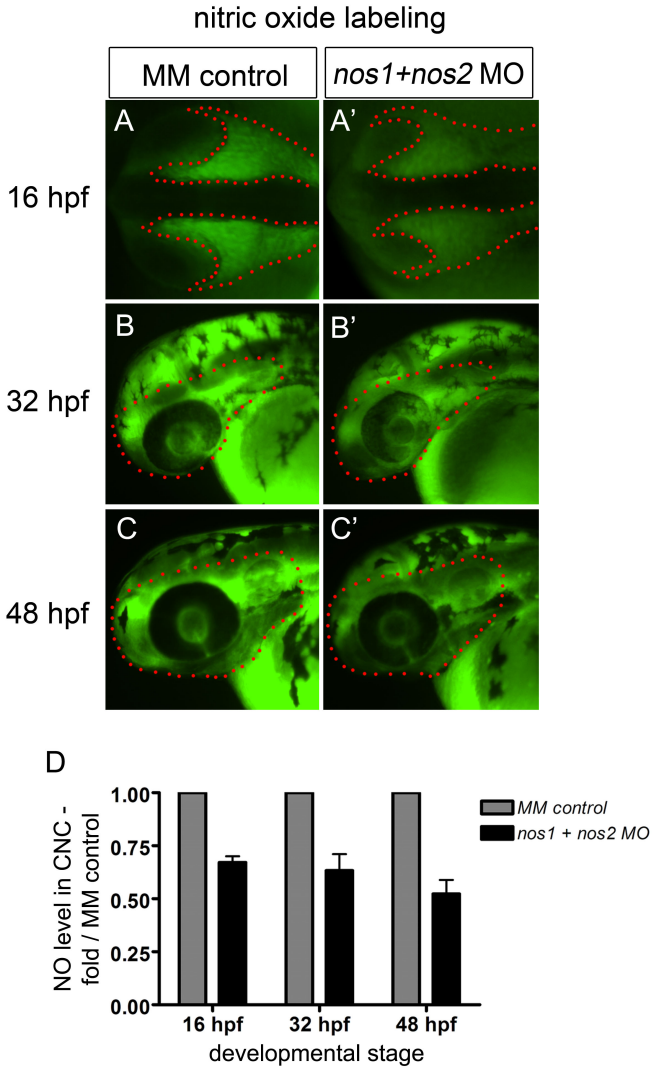

Figure S6. (Related to Figure 7) ***In vivo*** **nitric oxide levels in CNC and pharyngeal arches were decreased in** ***nos1+nos2*** **morphant during craniofacial development.** (**A-C, A'-C'**) Consistent decrease of *in vivo* NO signal was observed in *nos1+nos2* knockdown embryos compared with mismatch control at 16 hpf, 32 hpf, 48 hpf. (**D**) Quantification analysis of NO labeling in CNC and/or pharyngeal arches by fluorescent density.

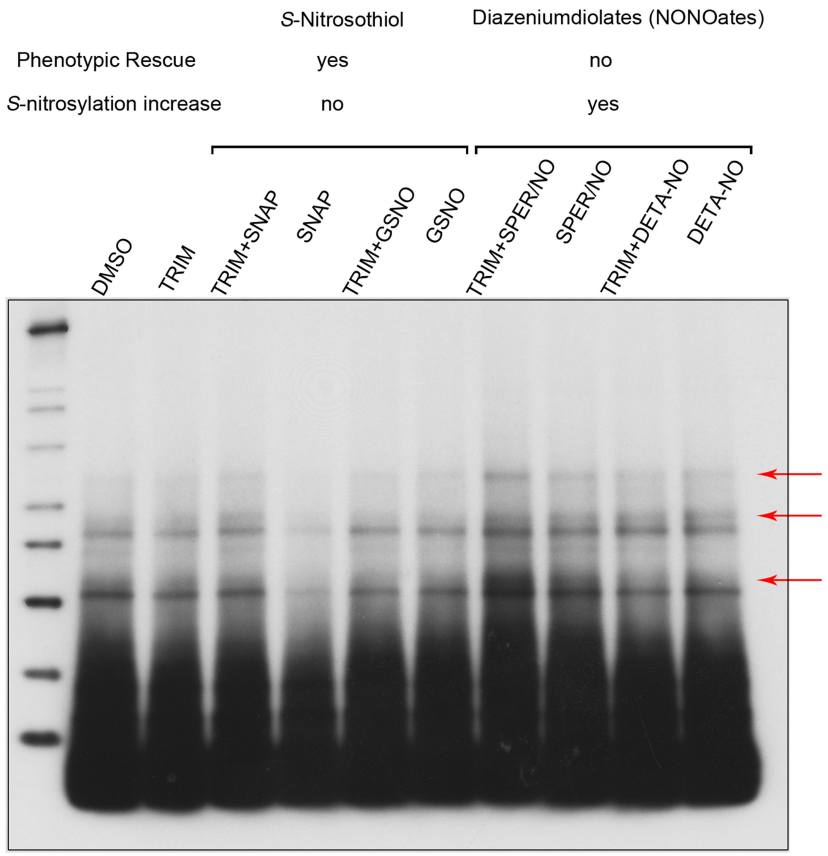

Figure S7. (Related to Figure 7) Changes in total S-nitrosylated proteins do not account for the rescued TRIM phenotype. Protein lysates were isolated from embryos treated with various chemical combinations as labeled. All samples were processed in biotin-switch assay for detection of protein S-nitrosylation. No significant difference was found in DMSO versus TRIM treated samples. Further, S-nitrosothiol class of NO donors (SNAP, GSNO), which were demonstrated in successful rescue of TRIM-induced craniofacial defect, did not lead to significant increase in protein nitrosylation. However, diazeniumdiolates (NONOates) class of NO donors (SPER/NO, DETA-NO), which were unable to rescue TRIM phenotype, were detected to stimulate the S-nitrosylated reaction of several proteins (red arrow), and served as positive controls for our biotin-switch assay.